Assessment of anisotropic damage in ASR-affected concrete structures by utilizing acoustic emission

Holthuizen, Patrick; Šavija, Branko; Çopuroğlu, Oğuzhan

DOI
10.58286/31721

Publication date
2025

Document Version
Final published version

Published in
e-Journal of Nondestructive Testing

NDT.net
e-Journal of Nondestructive Testing - ISSN 1435-4934 - www.ndt.net
eJNDT
NDT-CE 2025 - The International Symposium
on Nondestructive Testing in Civil Engineering
Izmir, Türkiye, September 24-26, 2025

Assessment of anisotropic damage in ASR-affected concrete structures by utilizing acoustic emission

Patrick E. HOLTHUIZEN[1], Branko ŠAVIJA[1], Oğuzhan ÇOPUROĞLU[1]

[1] Department of Materials & Environment, Faculty of Civil Engineering & Geosciences, Delft University of Technology, Delft, The Netherlands; p.e.holthuizen@tudelft.nl, b.savija@tudelft.nl, o.copuroglu@tudelft.nl

Abstract (*approx. 100 to 150 words*)
Assessing ASR damage through the elastic modulus (E-mod) is complicated due to the non-linear behaviour of cracked concrete, which can introduce testing artifacts. To address this, acoustic emission (AE) monitoring was applied during cyclic compression tests. AE data was used to define a critical load level, i.e. the maximum load at which no additional cracking occurred. By tracking high peak frequency events, it was possible to prevent high-energy AE signals associated with cracking. Limiting the loading below this threshold minimized test-induced damage. The stabilized secant E-modulus was then determined from subsequent cycles. This method resulted in E-modulus values 5–10% higher than after conventional testing. The load threshold varied with damage degree and crack orientation and is considerably lower than the commonly used load level at 40% of the compressive strength. These findings highlight the importance of AE-guided, damage-controlled testing protocols for reliable concrete mechanical performance assessment.

Keywords: Acoustic emission , Alkali-Silica reaction , Anisotropy , Damage assessment , Elastic modulus

1. Introduction

Older concrete infrastructure, originally designed for extended service life is widely relied upon today, often without adequate assessment of its current condition or the risks it may pose. Over time, such structures are subjected to various mechanical loads and degradation mechanisms. One particularly critical degradation process is the Alkali-Silica Reaction (ASR), which progressively damages the concrete quality throughout its lifespan [1,2].

An important indicator for ASR-related degradation is the reduction in the elastic modulus (E-modulus). The E-modulus is considered to be the most sensitive mechanical property to ASR-induced damage and is widely used to evaluate the extent of degradation [3,4]. However, using the modulus of elasticity as a practical assessment parameter is complicated if a reference value (for unaffected concrete) is unknown. Moreover, ASR-affected concrete exhibits nonlinear stress-strain behaviour even at low stress levels, in contrast to the linear elastic behaviour of undamaged concrete [5]. Interpreting stiffness degradation in ASR-affected concrete structures is additionally complicated due to the influence of internal stress state. Confinement conditions within a structure can introduce anisotropic stress fields, resulting in anisotropic expansion and damage. Consequently, an anisotropic stiffness reduction is observed for restrained specimens and is closely related to its expansion behaviour. The E-modulus reduces more in directions where the material is free to expand than in directions subjected to sustained loading [6].

This directional dependence in stiffness loss is dependent on the primary orientation and type of cracking. Cracks induced by ASR in confined conditions often exhibit preferential alignment, which in turn affects the elastic response of the material. When comparing specimens with cracks oriented perpendicular (horizontal) and parallel to loading (vertical), the difference in stiffness can be related to the closure of ASR-induced macro-cracks throughout the specimen. Once horizontally oriented cracks are closed in compression and loading reaches a sufficient level, there is a risk for inducing vertical splitting cracks. Consequently, the E-modulus will be additionally reduced [7]. This, in turn, implies that measured changes in E-modulus may not only reflect ASR damage but also include testing artifacts caused by load-

 https://doi.org/10.58286/31721

induced crack closure or splitting. Understanding both the stiffness reduction and the onset of nonlinearity is thus crucial for the development of accurate constitutive models [5]. Therefore, to isolate the effect of ASR from test-induced artifacts, it is essential to identify a critical load level below which only ASR-related damage affects the E-modulus, and no additional load-induced cracking occurs.

In this study, Acoustic Emission (AE) monitoring is employed to determine the appropriate load level for assessing the elastic modulus. During controlled loading-unloading sequences, AE waveforms were recorded to detect internal cracking events. Key AE-parameters, such as frequency, RA/AF ratio and cumulative AE energy, are frequently used to characterize rupture mechanisms and identifying the load level associated with the onset of cracking [8–12]. The critical threshold is identified by observing a change in registered AE waveforms, marked by a high frequency and a noticeable increase in cumulative AE energy. Specimens with varying damage levels and crack orientations were tested to capture the influence of anisotropy and degradation severity. By calculating the elastic modulus at the identified threshold load level, the study aims to isolate the effects of ASR-induced damage from load-induced artifacts. This approach enables a more accurate evaluation of anisotropic concrete stiffness degradation, especially in concrete cores with a horizontal preferential crack orientation.

2. Experimental program

2.1 Materials and sample preparation

This study investigates the damage in a post-tensioned concrete viaduct affected by ASR, through the evaluation of drilled core samples. The viaduct was constructed in the 1960s, using a concrete mixture with river dredged aggregates containing chert, a cement dosage of approximately 350 kg/m³ Ordinary Portland Cement and a design strength of 30 MPa. The structural system consists of columns supporting a cantilever slab, upon which prestressed beams are placed. ASR-induced damage was primarily observed on the underside of the slabs. A visual inspection confirmed varying degrees of damage across different slabs.

To quantify this damage, cores with a diameter of 104 mm and a length of 400 mm were extracted vertically (Z-direction) from several slabs. The coring direction was restricted to the least restrained direction, given that the structure is fully functional and post-tensioning was applied in the X and Y directions. After extraction, the cores were immediately wrapped in wet cloths and cling film to preserve moisture and were transported to the laboratory. The outer 50 mm of each core was removed, and the central portions were trimmed down to produce Ø104×200 mm test specimens to assess the E-modulus. Before testing, all samples were preconditioned for 48 hours in a humid curing room at 20 °C and 95%, following a procedure proposed by Sanchez et al. [13].

2.2 Methodology

2.2.1 X-ray computed tomography

X-ray computed tomography (X-ray CT) is employed to examine the internal damage and level of anisotropy within the three-dimensional microstructure of an extracted concrete core prior to mechanical testing. Cylindrical core specimens, measuring 104 mm in diameter and 200 mm in height, were scanned using the TESCAN CoreTOM high-resolution X-ray CT-scanner. Test specimens were tested in surface saturated condition. Specimens were removed from the curing room 30 minutes prior to scanning and wiped off with a dry cloth to remove excess surface moisture. The specimen was placed centered on a rotating table for scanning.

To ensure sufficient X-ray penetration through the test specimen, the X-ray tube was operated at an accelerating voltage of 200 kV and a beam current of 62 W. In order to improve the resulting tomogram and minimize artifacts, the produced X-ray beam was hardened by applying a 1 mm Sn-filter. Finally, by setting the Source-to-Surface Distance and the Source to Object Distance, a resolution of 62 µm per voxel was achieved. The scans produced approximately 3,000 projections with an exposure time per frame set to 325 ms. Each specimen was scanned in four sections, which were stitched using Panthera software to compile a complete 3D reconstruction. The resulting tomographic image stacks from the CT-scans were analysed using Dragonfly ORS software. A mean filter with a kernel size of 11 pixels was applied to each image slice to reduce noise and smooth the data, see Figure 1. Overall, this enabled the identification of coarse aggregates, the mortar fraction, cracks and pores.

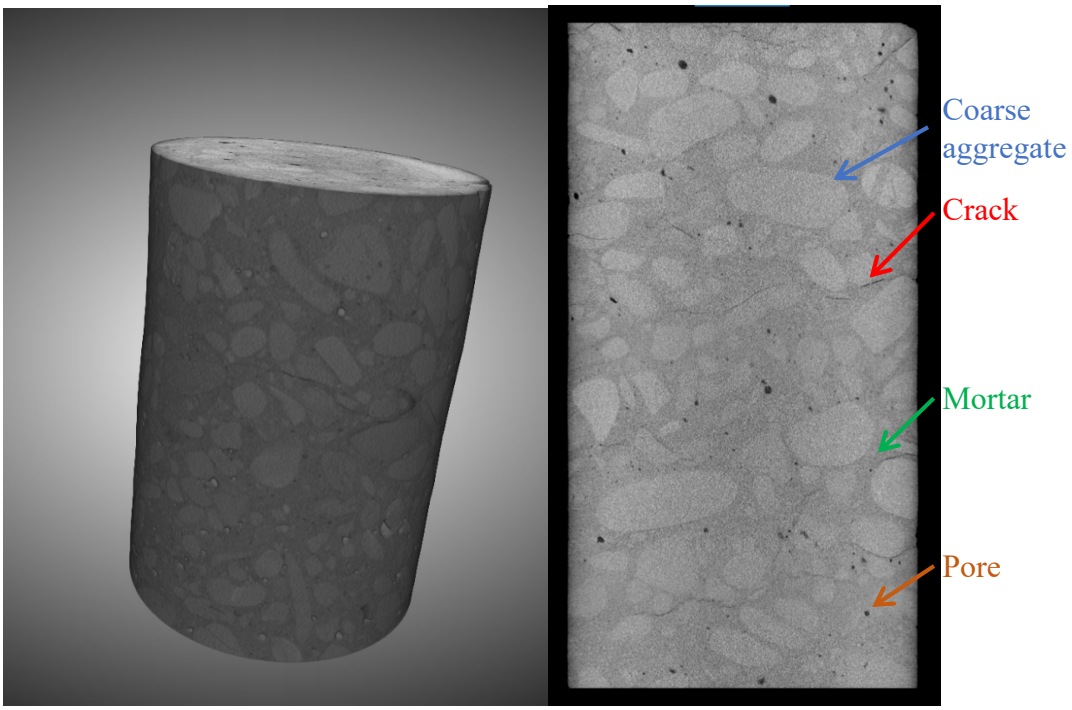

Figure 1. Reconstructed CT-scan of concrete core (left) and a tomogram of cross-section after filtering (right)

2.2.2 Elastic modulus

The secant modulus of elasticity in compression was determined on extracted concrete core using the Stiffness Damage Test (SDT). This cyclic test in compression is widely considered as a reliable method for assessing ASR-affected concrete structures [14]. The SDT procedure closely follows Method B for determining the E-modulus according to NEN-EN 12390-13 [15], which Sanchez et al. recommended when assessing ASR-related degradation in concrete [13]. Based on evaluation of the test output, calculating the secant modulus as the average of the second and third load–unload cycles provided the most consistent results. This approach proved effective up to 40% of the mix-design (28-day) compressive strength [13].

To ensure uniform load distribution, both ends of the concrete cores were mechanically ground to achieve flat and parallel surfaces. The test was conducted under load-controlled conditions using a hydraulic actuator with a maximum load capacity of 1500 kN. Test specimens with a diameter of 104 mm and a length of 200 mm were centrally positioned between two steel parallel loading plates. Four linear variable differential transformers

(LVDTs) were circumferentially and centrally placed over a length of 100 mm and used to measure the vertical strain. The specimens were subjected to a preload of 0.5 MPa, applied for no longer than 20 seconds. Deviations from NEN-EN 12390-13 were made regarding the loading rate and maximum applied load. Unlike the standard method, a loading rate of 0.1 MPa/s was used and the maximum applied load was adjusted based on the Acoustic emission monitoring. The applied load did not exceed 40% of the compressive strength (30MPa), which is equivalent to 12 MPa or 102 kN. The full loading sequence of the SDT consisted of five loading-unloading cycles, instead of three cycles according to the standard.

2.2.3 Acoustic emission

To record AE signals during the entire cyclic test, one wideband differential (WD) AE sensor (Mistras Group, Inc) was coupled with the specimen using hot melt adhesive, Figure 2. The operating frequency range of the used WD sensor was 100-900 kHz. A 32-channel Micro-II Express Digital AE system (Mistras Group, Inc) was employed for acquisition of the AE signals. Prior to acquisition the threshold was initialized at 45 dB and the sampling rate was set to 5 MHz. The hit definition parameters peak definition time (PDT), hit definition time (HDT) and hit lockout time (HLT) were set as 300, 600 and 1000 us, respectively. A band pass filter from 20 kHz to 1 MHz was used for the AE sensor. Finally, to assure sensor sensitivity and proper settings of the AE monitoring system, pencil-lead break tests [16] were conducted for each sensor before continuing with the main test. Waveforms of the received AE sensors were then saved for further analysis.

To reduce load-induced damage during testing, high peak frequency AE signals should be limited during testing and the loading level must be tailored to this [12]. We concluded that high peak frequency AE-signals would indicate the onset of small scale cracking and crack propagation. This previously developed criteria provide the onset for the current analysis by extending the damage evaluation to different degrees of damage. For the experiment, it was decided to allow a maximum of five peak frequency signals during the first load step, after which the corresponding load level was defined as the threshold.

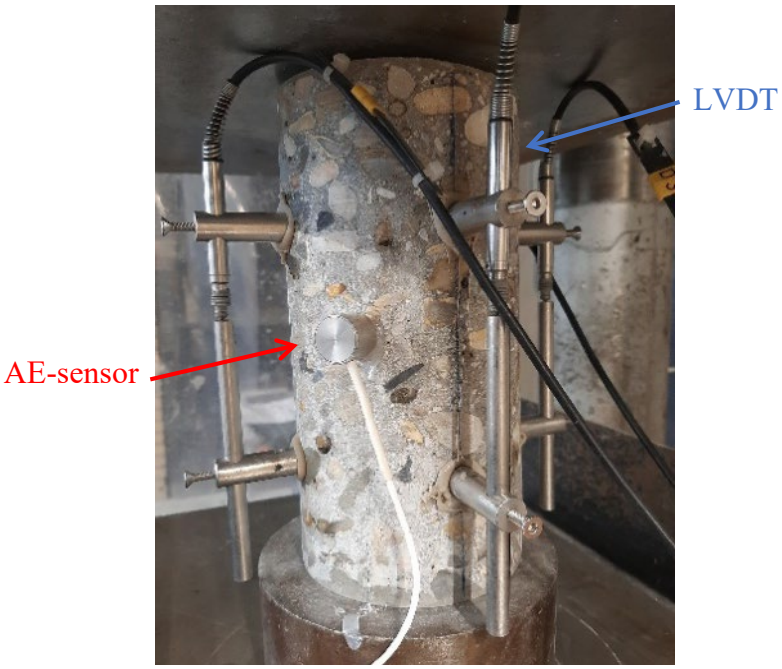

Figure 2. Placement of the LVDT's and AE-sensor for measurements during the SDT.

3. Results

3.1 Damage classification

After applying a mean filter in ORS Dragonfly, the tomograms were segmented using trainable Weka segmentation with an Image J plugin. A fast Random Forest (fRF) classifier was implemented, utilizing Gaussian blur, Sobel, Hessian, Difference of Gaussians (DoG) and membrane projection filters as training features. The fRF classifier generated 200 trees with a batch size of 100 using 16 threads and a membrane patch size of 19 pixels [17]. Weka segmentation was used to classify 4 different phases: background, pores, cracks and concrete (cement paste + aggregates). The resulting segmented images were then thresholded to highlight only the cracks and pores, as shown in Figure 3.

From Figure 3, a clear difference in the degree of damage can be seen, based on the different extent of cracking. As a result, of the voxel resolution and Weka segmentation, cracks as small as 62 µm could be identified. The tomogram on the right represents a less damaged (LD) specimen compared to the left, which is significantly more damaged (D). The LD specimen shows cracking primarily in the vicinity of coarse aggregates, without bridging cracks throughout the cement matrix, indicating a lower degree of ASR-induced damage. In contrast, the D specimen reveals greater anisotropic damage in the form of more horizontally oriented cracks that follow the outlines of aggregate particles.

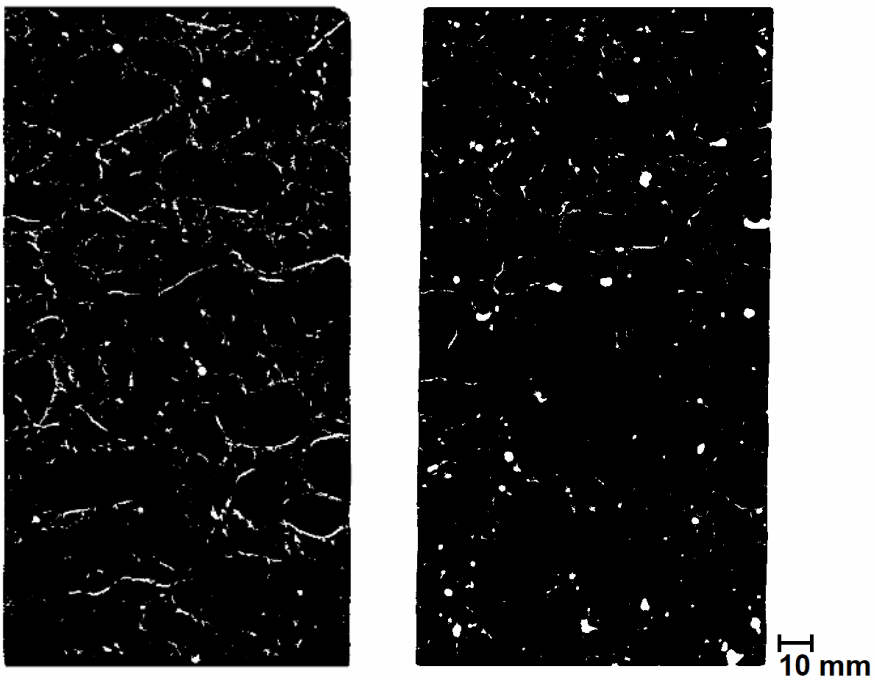

Figure 3. Segmented tomogram of crack and pores in (left) Damaged (D) and (right) less damaged (LD) samples

3.2 Acoustic emission monitoring

From Figure 4, it can be seen that by limiting the load to 80 kN, the cumulative AE energy release was reduced compared to the load of 102 kN and occurred solely during the first load step. While loading the damaged specimen, a load threshold of 80 kN was set after observing already five high peak-frequency signals during the first load step. In the following load-unload sequences, no more peak frequency signals were registered.

In contrast, when the specimen was subsequently loaded to 40% of its compressive strength, more than 20 of these peak frequency events were recorded, distributed over the entire

load-unload sequence. This resulted in nearly double the AE energy release compared to the threshold-load case. Additionally, the AE energy release occurred throughout the whole loading process rather than being confined to the initial load sequence. These results indicate that stopping the loading at the appointed threshold significantly limited the induced damage. The cumulative AE energy release was reduced to approximately one-third compared to the energy released when the specimen would be loaded directly to 40% of its compressive strength.

Furthermore, it should be noted that the LD specimen only exhibit one high peak-frequency signals upon reaching 40% load. The corresponding cumulative AE energy release was significantly lower compared to the damaged specimen, and it was considered that no additional damage was induced during loading. As a result, no load threshold was necessary, and the 40% load level was used to determine the E-modulus. The load sequence applied to the LD specimen until 40% load was identical to that used for the D specimen.

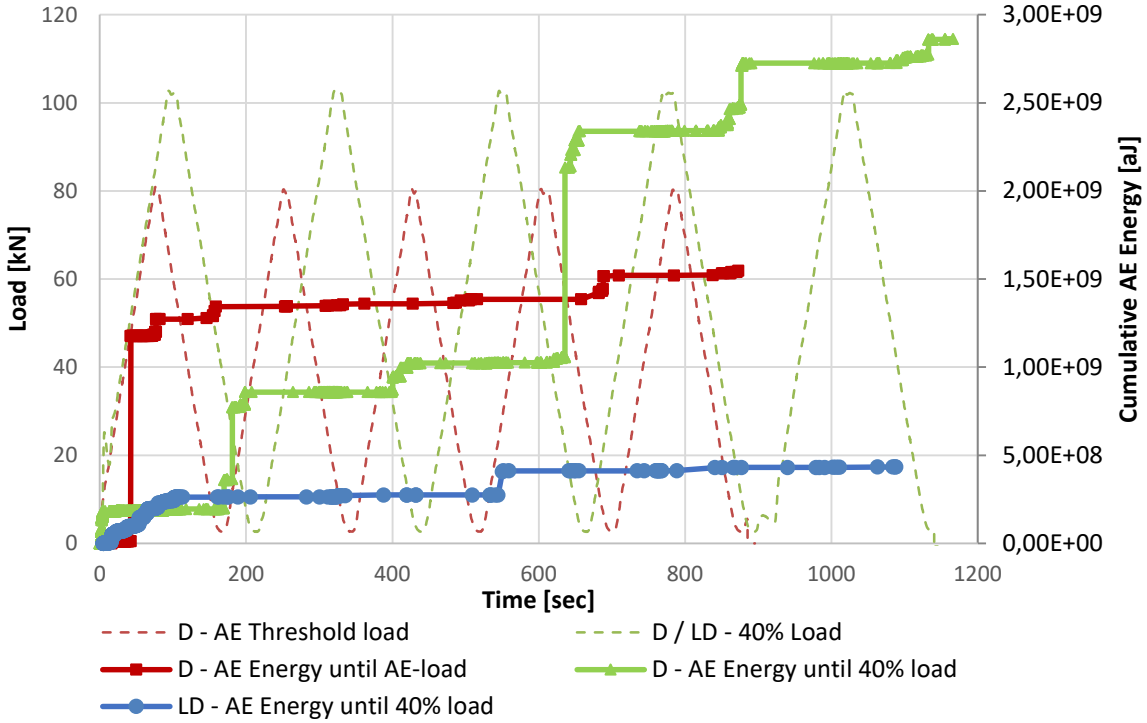

Figure 4. Cumulative AE-Energy release in relation to time and the loading sequence of the E-modulus

3.3 Modulus of elasticity

From the stress-strain curves presented in Figure 5, it can be seen that the first load step shows a slight non-linearity, appointed to pre-existing ASR-induced damage. As described in section 2.2.2., the secant modulus of elasticity is determined as the average of the second and third load–unload cycles. The modulus of elasticity determined for the different specimens, at their respective loading levels, is summarized in Table 1.

Based on the concrete design strength of 30 MPa, 40% of the cylindrical compressive strength corresponds to 12 MPa. Using cumulative AE energy monitoring, the load threshold was determined at 80 kN, which corresponds to a compressive stress of 9.5 MPa (31,5%). This means that by applying the threshold, the compressive load for the damaged specimen was reduced by approximately 10%.

For the damaged specimen, the modulus of elasticity was first determined at the threshold load. After completing the full load sequence at this level, the specimen was unloaded

and subsequently reloaded to 40% of the compressive strength. With this second loading sequence, the first load step displayed a slight concave shape, which can be attributed to the prior loading history at the threshold level. When comparing the damaged and less damaged specimens, it can be observed that the damaged specimen exhibits a higher strain. Consequently, this difference is also reflected in the calculated modulus of elasticity.

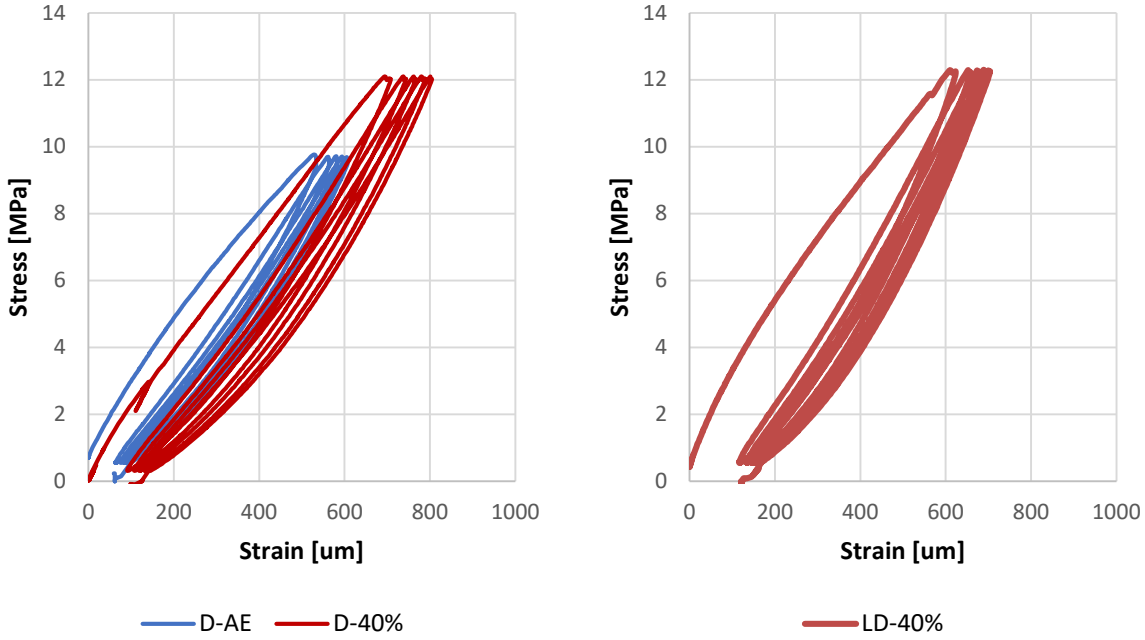

Figure 5. Stress-strain curves from the E-modulus test for specimens with different damage degrees due to ASR damage specimen (left) and less damaged (right)

The modulus of elasticity for the less damaged specimen is higher than that of the damaged specimen, which is related to the internal degree of damage, as visualized in Figure 3. Additionally, it can be observed that the elastic modulus determined at the AE threshold load is slightly higher than the value determined at 40% load. Based on the current experimental results, there is an additional reduction of approximately 5% in E-modulus that can be attributed to load-induced damage.

Table 1. Modulus of elasticity

Specimen type	E-modulus [GPa]
Damaged (D) – AE Load	19.5
Damaged (D) – 40% Load	18.3
Less Damaged (LD) – 40% Load	23.3

4. Discussion

The current experimental setup used only a single AE sensor, which offers a fast and simple means of detecting acoustic signals but has certain limitations. Notably, it cannot accurately localize AE sources within the concrete specimen due to wave attenuation effects. The registered AE waveform is affected by the mass of the concrete and its inherent damping effect. Consequently, it is possible that some AE events have occurred but are not clearly captured. When these events have been attenuated, it leads to an underreporting of the actual damage occurrence. The attenuation of AE signals in concrete can affect both the frequency and energy

content of the detected signals [18]. For instance, a high-frequency event occurring far from the sensor may appear as a low-frequency signal, and a high-energy event may register with much lower intensity. As such, AE parameters should be interpreted as indicators rather than absolute values. This raises concerns about using a fixed number of detected peak frequency signals to define a damage threshold. In the current study, the threshold load was determined after detecting five high-frequency AE events. However, considering the effects of attenuation and limited spatial coverage, it may be more appropriate to reduce this limit to two events to avoid underestimating early-stage damage.

In the damaged specimen, the stress–strain curve showed slight non-linearity around 5 MPa, coinciding with the detection of high-frequency AE signals and a noticeable increase in released AE energy. This behaviour may indicate the closure of horizontal cracks in the specimen with anisotropic damage. When the same specimen was reloaded to 40% of its compressive strength, the AE energy release approximately doubled. However, since damage had already occurred during the threshold loading, the difference in AE response between the two loading sequences is likely underestimated. This suggests that damage was already present at the threshold point, and that the measured E-modulus may already reflect a partially load-induced damaged state. Consequently, the actual ASR-affected E-modulus could be slightly higher than measured. This further underlines the importance of choosing a conservative AE threshold to avoid biasing the E-modulus measurement with early-stage damage.

A correct determination of the E-modulus is critical for practical assessment of ASR affected structures. Overestimating the reduction in E-modulus, even as little as 5–10%, can lead to an overestimation of the current damage degree and an underestimation of future degradation. Since the E-modulus is often used as an input parameter in constitutive models, inaccuracies can directly affect the predictive accuracy of structural assessments. Therefore, strengthening the methodology for determining the E-modulus of cracked concrete specimens is essential. Future work will focus on validating the AE load threshold using multiple sensors and refined criteria to improve the reliability of early damage detection.

5. Conclusion

This study investigated the use of acoustic emission (AE) monitoring to identify a load threshold and evaluate the E-modulus in ASR-affected concrete specimens. The main conclusions of this work are presented below.

- The use of AE-based thresholding proved effective in limiting additional load-induced damage during mechanical testing of concrete specimens. The use of AE to define a load threshold allowed testing to be paused before significant damage occurred.
- The attenuation of AE signals due to material and geometric effects reduces confidence in absolute parameter values. AE parameters should therefore be interpreted as indicators of damage evolution rather than absolute values.
- The E-modulus determined at the load threshold provides a more accurate representation of ASR-affected concrete stiffness. This demonstrates that the AE method helped reduce load-induced damage and provided a better estimate of the ASR-affected E-modulus.
- Accurate E-modulus determination is essential, as overestimating stiffness loss can affect the evaluation of current damage and future degradation. Future experiments should include multiple AE sensors to improve threshold accuracy and account for signal attenuation. This will help define more reliable and conservative AE-based load thresholds and strengthen confidence in E-modulus results for ASR-damaged concrete.

Acknowledgements

The authors would like to thank Yubao Zhou for providing the AE-sensors and assistance in setting up the AE acquisition system.

References

[1] R.N. Swamy, Assessment and Rehabilitation of AAR-affected Structures, Cem Concr Compos 19 (1997) 427–440.
[2] B. Fournier, M.A. Bérubé, Alkali-aggregate reaction in concrete: a review of basic concepts and engineering implications, Https://Doi.Org/10.1139/L99-072 27 (2011) 167–191. https://doi.org/10.1139/L99-072.
[3] R. Esposito, C. Anaç, M.A.N. Hendriks, O. Çopuroğlu, Influence of the Alkali-Silica Reaction on the Mechanical Degradation of Concrete, Journal of Materials in Civil Engineering 28 (2016) 04016007. https://doi.org/10.1061/(ASCE)MT.1943-5533.0001486.
[4] Institution of Structural Engineering, Structural effects of alkali-silica reaction, (1991). https://www.istructe.org/resources/guidance/structural-effects-alkali-silica-reaction/.
[5] S.S. Kongshaug, O. Oseland, T. Kanstad, M.A.N. Hendriks, E. Rodum, G. Markeset, Experimental investigation of ASR-affected concrete – The influence of uniaxial loading on the evolution of mechanical properties, expansion and damage indices, Constr Build Mater 245 (2020) 118384. https://doi.org/10.1016/J.CONBUILDMAT.2020.118384.
[6] A. Zahedi, C. Trottier, L. Sanchez, M. Noël, Evaluation of the induced mechanical deterioration of alkali-silica reaction affected concrete under distinct confinement conditions through the Stiffness Damage Test, Cem Concr Compos 126 (2022) 104343. https://doi.org/10.1016/J.CEMCONCOMP.2021.104343.
[7] S.G. Hansen, L.C. Hoang, Anisotropic Compressive Behaviour of Concrete from Slabs Damaged by Alkali-Silica Reaction, (2020). https://doi.org/10.1016/j.conbuildmat.2020.120377.
[8] F. Zhang, Y. Yang, S.A.A.M. Fennis, M.A.N. Hendriks, Developing a new acoustic emission source classification criterion for concrete structures based on signal parameters, Constr Build Mater 318 (2022) 126163. https://doi.org/10.1016/J.CONBUILDMAT.2021.126163.
[9] X. Song, X. Yu, W. Zhao, F. Yang, J. Shi, Ç. Yalçınkaya, Progressive damage process and destabilization precursor recognition of sulfate tailing-cemented paste backfill based on acoustic emission, Powder Technol 430 (2023) 119047. https://doi.org/10.1016/J.POWTEC.2023.119047.
[10] X. Liu, Z. Liu, X. Li, F. Gong, K. Du, Experimental study on the effect of strain rate on rock acoustic emission characteristics, International Journal of Rock Mechanics and Mining Sciences 133 (2020) 104420. https://doi.org/10.1016/J.IJRMMS.2020.104420.
[11] S. Fotouhi, M. Assaad, M. Nasor, A. Imran, A. Ashames, M. Fotouhi, Multivariable Signal Processing for Characterization of Failure Modes in Thin-Ply Hybrid Laminates Using Acoustic Emission Sensors, Sensors 2023, Vol. 23, Page 5244 23 (2023) 5244. https://doi.org/10.3390/S23115244.
[12] P. Holthuizen, Y. Zhou, B. Šavija, O. Çopuroğlu, Evaluation of the Non-destructive Character of the Stiffness Damage Test for Damage Assessment of Concrete Structures

Affected by Alkali-Silica Reaction Using Acoustic Emission, RILEM Bookseries 50 (2024) 3–10. https://doi.org/10.1007/978-3-031-59349-9_1.
[13] L.F.M. Sanchez, B. Fournier, M. Jolin, J. Bastien, Evaluation of the Stiffness Damage Test (SDT) as a tool for assessing damage in concrete due to alkali-silica reaction (ASR): Input parameters and variability of the test responses, Constr Build Mater 77 (2015) 20–32. https://doi.org/10.1016/j.conbuildmat.2014.11.071.
[14] T.M. Chrisp, P. Waldron, J.G.M. Wood, Development of a non-destructive test to quantify damage in deteriorated concrete, Magazine of Concrete Research 45 (1993) 247–256. https://doi.org/10.1680/MACR.1993.45.165.247.
[15] NEN-EN 12390-13:2021, Testing hardened concrete - Part 13: Determination of secant modulus of elasticity in compression, CEN (2021).
[16] N. Hsu, F. Breckenridge, Characterization and calibration of acoustic emission sensors, Material Evaluation 39 (1981) 60–68.
[17] L. Breiman, Random forests, Mach Learn 45 (2001) 5–32. https://doi.org/10.1023/A:1010933404324/METRICS.
[18] Y. Zhou, B.B. Aydin, F. Zhang, M.A.N. Hendriks, Y. Yang, A lattice modelling framework for fracture-induced acoustic emission wave propagation in concrete, Eng Fract Mech 312 (2024) 110589. https://doi.org/10.1016/J.ENGFRACMECH.2024.110589.